THE JOURNAL OF BIOLOGICAL CHEMISTRY
Vol. 277, No. 37, Issue of September 13, pp. 34489–34498, 2002

Printed in U.S.A.

Structural Basis for the NAD-dependent Deacetylase Mechanism of Sir2*

Received for publication, June 3, 2002, and in revised form, June 27, 2002
Published, JBC Papers in Press, June 28, 2002, DOI 10.1074/jbc.M205460200

Jeong-Ho Chang, Hyun-Chul Kim, Kwang-Yeon Hwang, Joon-Won Lee, Stephen P. Jackson‡, Stephen D. Bell§, and Yunje Cho¶

From the National Creative Research Initiative Center for Structural Biology and Department of Life Science, Pohang University of Science and Technology, Hyo-ja dong, San31, Pohang, KyungBook 790-784, South Korea, ‡Wellcome Trust/Cancer Research United Kingdom Institute of Cancer and Developmental Biology, Tennis Court Rd., Cambridge, CB2 1QR, United Kingdom, and §Medical Research Council Cancer Cell Unit, Hills Rd., Cambridge, CB2 2XZ, United Kingdom

The NAD-dependent histone/protein deacetylase activity of Sir2 (silent information regulator 2) accounts for its diverse biological roles including gene silencing, DNA damage repair, cell cycle regulation, and life span extension. We provide crystallographic evidence that 2′-*O*-acetyl ADP-ribose is the reaction product that is formed at the active site of Sir2 from the 2.6-Å co-crystal structure of 2′-*O*-acetyl-ADP-ribose and Sir2 from *Archaeoglobus fulgidus*. In addition, we show that His-116 and Phe-159 play critical roles in the catalysis and substrate recognition. The conserved Ser-24 and Asp-101 contribute to the stability for NAD binding rather than being directly involved in the catalysis. The crystal structures of wild type and mutant derivatives of Sir2, in conjunction with biochemical analyses of the mutants, provide novel insights into the reaction mechanism of Sir2-mediated deacetylation.

Sir2 is a novel histone deacetylase that removes acetyl groups from acetylated lysine residues only in the presence of NAD (1–4). In addition, Sir2 possesses weak ADP-ribosyltransferase activity (5). The deacetylation activity of Sir2 contributes to its transcriptional silencing activity at the telomeric, ribosomal DNA, and silent mating type loci in yeast and contributes to the cellular aging processes of *Saccharomyces cerevisiae* and *Caenorhabditis elegans* (6–11). In addition to gene silencing, Sir2 helps to mediate DNA repair of double-stranded DNA breaks (12).

Recently, it has been shown that the biological function of Sir2 is not restricted to transcriptional silencing and DNA double strand break repair. First, Sir2 homologues with NAD-dependent protein/histone deacetylase activity are found in several bacteria and Archaea that do not possess histones (13). Indeed, recent work has demonstrated that an archaeal Sir2 homologue deacetylates the archaeal non-histone chromatin protein, Alba, and thereby modulates its DNA binding affinity (14). Second, there are multiple Sir2 homologues in eukaryotes. For instance, there are at least seven and five Sir2 homologues in humans and yeast, respectively (13). Third, eukaryotic Sir2 homologues have a broad substrate specificity that allows them to remove acetyl groups from non-histone proteins including p53 and bovine serum albumin (BSA)[1] (15–17). It has been shown that human Sir2, SirT1, represses p53-dependent apoptosis upon DNA damage and oxidative stress by deacetylating p53 (15, 16). Finally, in *Arabidopsis*, the inhibition of a Sir2 homologue results in atypical body axis formation and vascularization (18). In addition, the product of Sir2, *O*-acetyl ADP-ribose, has been shown to delay or block the cell cycle in embryonic development (19). Thus, it is of considerable interest to understand how Sir2 removes an acetyl group from its acetylated lysines in its protein substrates, transfers the acetyl group to NAD, and forms the final product, *O*-acetyl ADP-ribose, which could be an important metabolite in cell signaling.

Two Sir2 crystal structures have been reported recently, namely Sir2 from *Archaeoglobus fulgidus* bound to NAD (Sir2-Af1) and the catalytic core of human SirT2 (17, 20). Furthermore, a mass spectrometry analysis indicates that 1′-*O*-acetyl ADP-ribose could be the final product of Sir2 reaction (21). On the basis of these and other biochemical studies, several catalytic mechanisms for Sir2 have been proposed (21, 22). Although all the proposed mechanisms include the hydrolysis of the high energy bond between nicotinamide and ADP-ribose followed by formation of an acetate-ADP-ribose intermediate to produce *O*-acetyl-ADP-ribose, the detailed reaction mechanism is ambiguous. Furthermore, the individual roles of the Sir2 active site residues during catalysis are unclear. For instance, it has been proposed that Sir2 may function like a serine protease in that a conserved serine residue could act as a catalytic base in the cleavage of the glycosidic linkage in nicotinamide ribose (17). However, this residue is far from the cleavage site and buried within the core of the protein. More importantly, the identity of the true product of Sir2 reaction is unclear since mass spectrometric analysis cannot distinguish the position of the acetyl group within the nicotinamide ribose. Indeed, the regio-isomer of 2′- and 3′-*O*-acetyl ADP-ribose has recently been proposed as the final product of the Sir2 catalyzed reaction on the basis of NMR studies (23, 24)

To understand the NAD-dependent deacetylase mechanism more clearly, we have carried out structural and functional studies on Sir2 homologues from *A. fulgidus* (Sir2-Af1). *A. fulgidus* is a sulfur-metabolizing hyperthermophile with an optimum growth temperature at 83 °C (25). The entire genome

* This work was supported by National Creative Research Initiatives program, Frontier 21 program, and a KAST young scientist award in life science (to Y. C.). The costs of publication of this article were defrayed in part by the payment of page charges. This article must therefore be hereby marked "*advertisement*" in accordance with 18 U.S.C. Section 1734 solely to indicate this fact.

The atomic coordinates and structure factors (code 1M2G, 1M2H, 1M2J, 1M2K, and 1M2N) have been deposited in the Protein Data Bank, Research Collaboratory for Structural Bioinformatics, Rutgers University, New Brunswick, NJ (http://www.rcsb.org/).

¶ To whom correspondence should be addressed. Tel.: 8254-279-2288; Fax: 8254-279-8111; E-mail: yunje@postech.ac.kr.

[1] The abbreviation used is: BSA, bovine serum albumin.

sequence of *A. fulgidus* has been recently determined, and the genomic DNA analyses reveal that two Sir2 homologues, Sir2-Af1 and Sir2-Af2, are present in this Archaea bacterium (26). The Sir2 from *S. cerevisiae* share sequence identity of 24 and 27% with Sir2-Af1 and Sir2-Af2, respectively. Biochemical studies confirm that these proteins have NAD-dependent protein deacetylase activities; the Sir2-Af1 deacetylates the acetyl group from the acetylated BSA, whereas Sir2-Af2 removes the acetylated N-terminal tail of histone (2, 17). Here, we have undertaken an analysis of the enzymatic and structural consequences of mutagenesis of active site residues to elucidate the catalytic mechanism of Sir2-Af1. In addition, we provide direct crystallographic evidence that 2′-*O*-acetyl ADP-ribose is formed in the active site as a result of the catalytic reaction.

EXPERIMENTAL PROCEDURES

Expression and Purification—The reported Sir2-Af1 sequence was used to construct two oligonucleotide primers (primer 1, CATGCTAGGGGATCCATGGACGAAAAACTGTTGAAA; primer 2, TCGCATGAGAAGCTTTAAAGACAGAGCTTTCCTGAC) that were used in a PCR to amplify Sir2-Af1 from purified *A. fulgidus* chromosomal DNA (26). The amplified fragment was restricted using *Bam*HI and *Hin*dIII and subcloned into pQE-30 vector. The entire Sir2-Af1 was sequenced to confirm that no mutation occurred during the PCR. We found that the stop codon was mutated to Leu during the PCR reaction, resulting in the introduction of four extra residues, Leu-Lys-Leu-Asn, at the C terminus. All the mutants reported here were generated by PCR-based methods using the appropriate primers, and the mutation was verified by DNA sequencing. During the course of PCR, a mutant where three residues (D102G/F159A/R170A) were mutated was also generated. For the convenience, we named this one as a triple mutant throughout the text. The plasmid containing wild type or mutant Sir2 gene was transformed into XL1Blue, and the cell was grown in LB media containing 100 μg/ml ampicillin until an A_{600} of 0.6 was reached before induction with 0.2 mM isopropyl-1-thio-β-D-galactopyranoside for 4 h.

The N-terminal His-tagged proteins were purified as suggested (Qiagen). Briefly, cells were harvested by centrifugation and lysed by sonicator in 50 mM NaH_2PO_4, pH 8.0, 300 mM NaCl, 10 mM imidazole, and 1 mM 2-mercaptoethanol. The lysate was clarified by centrifugation and incubated at 80 °C for 1 h. The mutant proteins were purified by nickel column instead of heat treatment. The imidazole gradient with solutions containing 20–250 mM imidazole in 50 mM NaH_2PO_4, pH 8.0, 300 mM NaCl, and 1 mM 2-mercaptoethanol was applied to the column. The eluted proteins were further purified using Mono-S by NaCl gradient (0–500 mM) and, finally, by gel filtration equilibrated with buffer containing 10 mM Tris-HCl, pH 8.0, 200 mM NaCl, and 5 mM dithiothreitol. The proteins were finally concentrated to 20 mg/ml by ultrafiltration and stored at −70 °C until use.

Crystallization and Data Collection—All the crystals used in this study were obtained by the hanging drop vapor diffusion method. Concentrated proteins were initially mixed with NAD to a final concentration of 5 mM and incubated for 30 min at 4 °C before crystallization. The monoclinic form of crystals was obtained by mixing the protein solution with an equal volume of the buffer used in the crystallization well (100 mM sodium citrate, pH 6.0, 14% polyethylene glycol 4000 and 20% isopropanol) and equilibrated with 1 ml of reservoir solution at 18 °C. Crystals with a size of 0.05 × 0.2 × 0.3 mm appeared within 2–3 days.

Hexagonal I form crystals were obtained from a buffer containing 100 mM HEPES, pH 7.5, and 13–18% polyethylene glycol 8000. Incubation of hexagonal I form crystals with 500 mM *N*-acetyl lysine, 100 mM HEPES, and 13–18% polyethylene glycol 8000 at 18 °C for 4–5 days resulted in an alteration of the unit cell dimensions and space group to the hexagonal II form. The detailed statistics are summarized in Table I. An asymmetric unit of the monoclinic form contains a single molecule, and an asymmetric unit of the hexagonal form contains two molecules.

All data were measured at −190 °C using a flash-frozen crystal on a RaxisIV image plate system mounted on a Rigaku RU-200 rotating anode x-ray generator or at beamline B6 at Pohang accelerated light source. Determination of unit cell parameters and integration of reflections was performed using the program DENZO (27) from the HKL package. Data were scaled and merged with SCALEPACK (27).

Model Building and Refinement—The structure of each crystal was solved by molecular replacement using the AMORE with diffraction data in the 15–4-Å resolution range (28). In each case, the initial R factor for the molecular replacement solution was 37–38% for all the data lower than or equal to 3.0-Å resolution. With a correctly positioned model, $F_o - F_c$ and $2F_o - F_c$ maps were calculated, and manual adjustment of the model was performed using the programs CHAIN and O (29, 30). The model was further refined using CNS with Engh and Huber stereochemical parameters (31). Refinement statistics are presented in Table I.

Enzymatic Assays—The deacetylase activity of Sir2-Af1 was measured by detecting the release of [^{3}H]acetate from ^{3}H-acetylated BSA using a reported protocol (17). In short, 2 μg of purified Sir2 proteins were incubated with 50 μg of [^{3}H]acetyl-labeled BSA for 60 min at 50 °C in buffer containing 50 mM citrate, pH 6.0, 5 mM $P_2O_7^{4-}$, 500 μM NAD, 500 mM NaCl, and 1 mM dithiothreitol. The reaction was stopped with 50 μl of 1 M HCl and 400 mM acetic acid. The released ^{3}H product was extracted with ethyl acetate and counted in a scintillation counter.

Enzyme Kinetics—Reaction mixtures containing 50 mM citrate, 500 μM NAD, 500 mM NaCl, 1 mM dithiothreitol, and 0.37–1.48 μM enzyme were incubated at 50 °C. The acetylated BSA (5–200 μM final concentration) were added to the mixture, and the amount of [^{3}H]acetate from [^{3}H]acetylated BSA was measured at various temperatures and times. The K_m and k_{cat} values were determined by Lineweaver-Burk plots using the ENZFITTER data analysis program (32).

Stability Measurement—Conformational changes for each protein (55.5 μM) were monitored at various temperatures by scanning with a circular dichroism spectrometer (Jasco J-715). The temperature was raised from 40 to 110 °C over a 70-min period, and detection was set on 222 nm. Measured data fitting was performed using Sigma-plot 2000.

Measurement of NAD Binding—Binding constants of the NAD to wild type and mutant Sir2 were measured by isothermal titration calorimetry using the Micro Calorimetry system (MicroCal). Purified Sir2 was extensively dialyzed against buffer containing 150 mM NaCl, 1 mM dithiothreitol, and 20 mM Tris-HCl, pH 8.0, before binding assay. Briefly, 4.5 mM NAD in the same buffer was titrated into a 0.13–0.23 mM solution of Sir2 protein at 40 °C. Titration curves, typically consisting of 20 points, were fitted to the two-state binding model using the program ORIGIN (MicroCal).

RESULTS AND DISCUSSION

Crystallization and Overall Structure—Initially, we obtained a hexagonal form of crystals of Sir2-Af1 by use of the hanging drop vapor diffusion method from a solution containing 100 mM sodium citrate, pH 6.0, 20% polyethylene glycol 4000, and 15–20% isopropanol at 4 °C. This crystal belongs to the space group of $p6_5$, with dimensions of $a = b = 45.5$ Å and $c = 235.5$ Å and diffracted to 2.7-Å resolution at spring 8 synchrotron station. The structure of the crystal was determined by the method of multiwave anomalous diffraction to 2.7 Å using Zn^{2+} as an anomalous scatterer (data not shown). The map generated from the multiwave anomalous diffraction phases was excellent in most of the regions, and we were able to build the complete model and NAD on the experimental map. However, the resulting model did not refine well for unknown reasons and produced poor refinement statistics; the final R-factor and R-free were 26.5 and 36.5%, respectively, and only 68% of total residues fell in the most favorable regions in a Ramachandran plot. This partially refined structure was virtually identical to the open form structure of Sir2-Af1 reported by Min *et al.* (17). Refinement using the structure from Min *et al.* (PDB code 1ICI) did not improve the statistics or the quality of the model (see below for the overall structure).

We then adjusted the crystallization conditions as described under "Experimental Procedures," and this change together with the extra four residues introduced at the C terminus as the result of the PCR reaction, used to produce Sir2-Af1, altered the packing of the molecules and yielded a monoclinic form of a crystal. This had a significantly improved diffraction limit, and the crystal diffracted to 1.47-Å resolution. In addition, we also crystallized a triple Sir2 mutant (D102G/F159A/R170A). This resulted in the formation of a hexagonal form I crystal that was different from our original crystal (Table I). Finally, hexagonal form II was obtained by performing the crystallization in the presence of *N*-acetyl lysine (see "Experimental Procedures" for details).

TABLE I
Statistics from crystallographic analysis

$R_{sym} = \Sigma_h\Sigma_i|I_{h,i} - I_h|/\Sigma_h\Sigma_i I_{h,i}$, where I_h is the mean intensity of the i observations of symmetry-related reflections of h. $R = \Sigma||F_{obs}| - |F_{calc}||/\Sigma|F_{obs}|$, where $F_{obs} = F_p$, and F_{calc} is the calculated protein structure factor from the atomic model (R_{free} was calculated with 5% of the reflections). Root mean square deviation (r.m.s.d.) in bond lengths and angles are the deviations from ideal value.

	Wild type	S24A	H80N	F159A	Triple (I)	Triple (II)
Data set						
Resolution (Å)	50–1.7	40–1.8	40–1.7	50–1.47	50–2.8	50–2.6
Space group	$P2_1$	$P2_1$	$P2_1$	$P2_1$	$P3_2$	$P3_121$
A	35.11	35.71	35.68	35.92	84.04	84.72
B	84.76	85.29	85.55	85.51	84.04	84.72
C	44.74	44.85	44.79	44.86	95.92	193.09
β	109.21	112.08	111.99	112.35	–	–
Total observations	87707	60264	70651	98112	87520	81444
Unique observations	26195	21671	24483	36883	14038	19629
Data coverage (%)	94.8	93.8	89	88.0	75.3	77.3
R_{sym}	3.1	3.2	3.8	3.1	6.4	5.3
Mean I/σ (I)	42.5	26.2	18.8	31.2	18.3	16.2
Refinement						
Resolution range	40–1.7	40–1.8	40–1.7	40–1.47	40–2.8	40–2.6
Number of reflections (I > 0)	26173	21668	24436	36847	14031	19681
$R_{working}$	18.91	18.99	18.22	20.47	22.90	22.89
R_{free}	22.02	21.67	21.83	23.10	32.81	30.6
Number of protein atoms	1942	1941	1940	1936	3839	3850
Number of water/ligand/ion atoms	260/36/1	277/36/1	285/36/1	347/36/1	0/72/2	158/78/2
r.m.s.d. bond length (Å)	0.005	0.005	0.005	0.005	0.01	0.008
r.m.s.d. bond angles (°)	1.23	1.19	1.22	1.16	1.74	1.50
r.m.s.d. for bonded main chain atom	1.29	1.19	1.16	1.28	1.26	1.35

The overall structure of the protein consists of two domains, a large domain with an α/β or Rossman fold composed of six α-helices and six parallel β-strands and a small domain with three antiparallel β-strand, two α-helices, and a zinc atom (Fig. 1*a*). When the structures of monoclinic and hexagonal (I) forms were compared with the open form of Sir2, most of the regions were very similar, showing root mean square deviations of 1.6 Å (monoclinic form) to 1.3 Å (hexagonal I form) for all Cα atoms. However, significant differences were observed in the loop region (located from residues 29 to 48) that is situated over the NAD binding site. When the loop segment alone was compared with that of open form, the root mean square deviations for Cα atoms were 4.5 Å (monoclinic form) and 3.2 Å (hexagonal I form). The electron density in the loop region is well defined in all three crystal forms, and the average temperature factor in this region is similar to that of the whole molecule. Nevertheless, the notable conformational differences in the loop segment of different crystal forms indicate that this is most flexible region in the molecule (Fig. 1*a*).

In the monoclinic form, residues 30–34 in the loop were closer to the active site than the equivalent regions in the open form, whereas residues 41–48 were slightly further away from the active site. The most noticeable movement included the rearrangement of the positions of Phe-32 (7 Å), Arg-33, and Trp-39 (14 Å) toward the nicotinamide ribose in the active site (Fig. 1, *b* and *c*). Because several residues in the loop more tightly surround NAD in the active site, the monoclinic form adopts a "closed" loop conformation relative to the open form.

In both hexagonal I and II forms, the loop segment in the hexagon forms intermediate conformations between the open and closed form; residues 30–33 adopted conformations more similar to the closed form, whereas the conformations of residues 38–48 were more similar to the open form.

Active Site—Although an excess of NAD was added to Sir2 before crystallization, we observed only the ADP-ribose density in the monoclinic form and not the NAD density (Fig. 1*b*). It is possible that the nicotinamide ring in this structure was disordered and, therefore, not visible. However, several lines of evidence suggest that this was not the case. First, the hydroxyl group linked to C1′ of nicotinamide ribose was tightly packed by the surrounding residues, and there was insufficient space to accommodate the nicotinamide ring. Second, the high resolution electron density clearly showed that the bound ligand was an α-form, whereas the NAD we added was a β-form. Thus, we presume that during the crystallization, β-NAD was converted to ADP-ribose. In contrast to the monoclinic crystals, the active site in hexagonal form I crystals contained enough space for the nicotinamide ring to fit in. Furthermore, in the hexagonal form 1 crystals, the ADP-ribose was still in the β-form. We assume therefore, that NAD was bound in this crystal form. However, we did not observe the nicotinamide ring, and thus, we presume that if it was indeed present, it was disordered.

The ADP-ribose bound to the active site of Sir2 in a similar manner to that described for NAD (17) in that it was oriented in an inverted direction compared with most other NAD-binding proteins. In general, ADP-ribose binds extensively to a pocket formed by several conserved residues at the interface between the large and small domains of NAD-binding proteins. Previously, the NAD binding site in Sir2-Af1 was divided into three sites, site A for binding of adenine ribose, site B for binding of nicotinamide ribose, and site C, which does not make any direct interaction with NAD but forms a core inside the pocket. This provides local stability to the residues that interact with the adenine ribose and phosphate moiety. In the three different crystal forms we studied, the interactions between the pocket residues and the ligand in site A were highly conserved. The adenine base was surrounded by residues Gly-22, Ala-25, Gly-185, Pro-212, and Lys-228, and the adenine base and ribose made a direct hydrogen bond to the main or side chains of Glu-26, Asn-211, Asp-213, and Ala-229.

The interactions between residues in site C were also conserved in all the crystal forms. Ser-24 formed direct hydrogen bonds with His-80 and Asp-101 (Fig. 1*c*). A buried water molecule mediated the interactions in Ser-24, His-80, Asn-99, and Asp-101. Large fractions of the side chains in these residues were buried. The fractional accessible surface area for the side chains of these residues was 2% for Ser-24, 7% for Asn-99, 6% for Asp-101, and 0% for His-80.

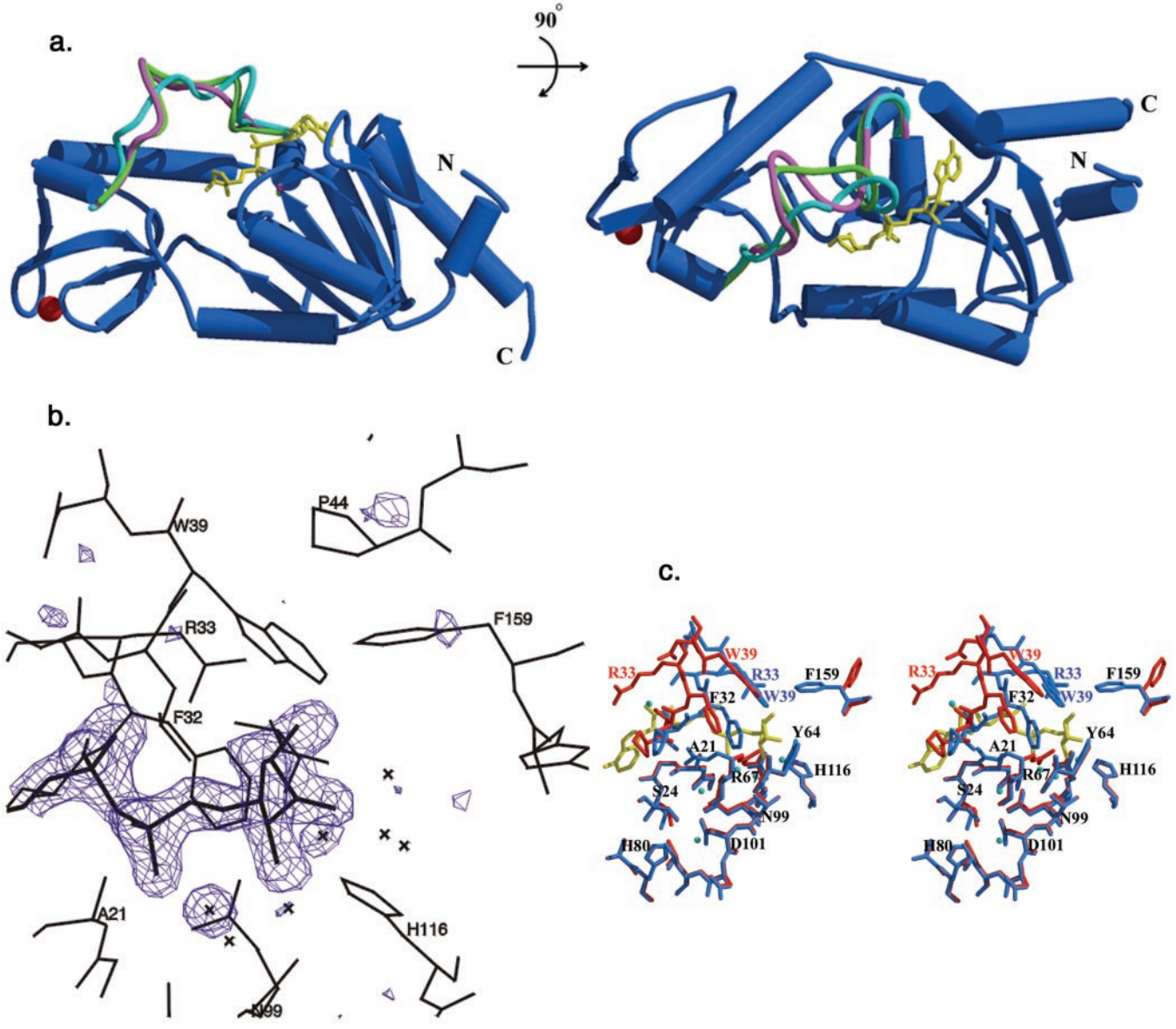

FIG. 1. *a*, the overall structure of the Sir2-Af1 and ADP-ribose complex determined at 1.7 Å is shown in two different views using ribbon representation. Three different conformations of a flexible loop comprising residues 29–48 are superimposed and colored *blue* (closed or monoclinic form), *green* (open or hexagonal form), and *magenta* (intermediate or hexagonal I/II) form. The zinc ion is colored *red*, and ADP-ribose is *yellow*. The figures were drawn with the programs MOLSCRIPT (34) and RASTER3D (35). *b*, the 1.7-Å $F_o - F_c$ map showing the region around the ADP-ribose. The map is contoured at the 3σ level. *c*, stereo view of the ADP-ribose binding pocket containing sites A, B, and C in the open (*blue*) and closed form (*red*). Arg-33 and Trp-39 are leveled in both forms with different colors to show the conformational changes more clearly. ADP-ribose is shown in *yellow*.

The most significant differences between the structures derived from the different crystal forms were observed in the interactions in site B as a result of the closure of the flexible loop (Fig. 1*c*). The O1′ of nicotinamide ribose made hydrogen bonds with NE of Trp-39 and NH1 from Arg-33. The NH1 group of Arg-33 also interacted with O_2'A and O4′ of nicotinamide ribose. The aromatic ring of Phe-159 was about 3.4 Å away from O1′ of the ribose ring. Side chains of Phe-32 and Val-190 were also close to the ribose ring. The OH3′ of ribose made a hydrogen bond to ND1 of His-116. The ribose ring adopted the C2′ exo conformation rather than the C3′ endo conformation seen in the open form.

It is unclear why ADP-ribose was observed instead of NAD. It is possible that the weak ADP-ribosyltransferase activity of Sir2 may lead to the cleavage. However, ADP-ribose instead of NAD was also seen in some mutant structures such as Ser-24, in which the ADP-ribosyltransferase activity is almost abrogated (data not shown, see below). Furthermore, the NAD-dependent deacetylation reaction occurred between NAD and excess *N*-acetyl lysine in hexagonal I form (see below). Thus, formation of ADP-ribose may be due to the crystallization conditions facilitating hydrolysis of the relatively unstable glycosidic bond between nicotinamide and ribose.

Catalytic Residues—On the basis of structural and sequence conservation, we carried out mutational studies on Sir2-Af1 to identify the functional residues that are involved in catalysis (Fig. 2). Our data show that the Arg-33 to Ala mutant retained about 80% activity, suggesting that the interactions between Arg-33 and nicotinamide ribose contribute little to catalysis. Glu-45 does not interact with NAD directly, and its mutation did not affect the activity. Strikingly, however, replacement of His-116 with Asn/Asp and Phe-159 with Ala significantly affected the deacetylation activity. and therefore, these residues are likely to be involved in the enzyme reaction. Specifically,

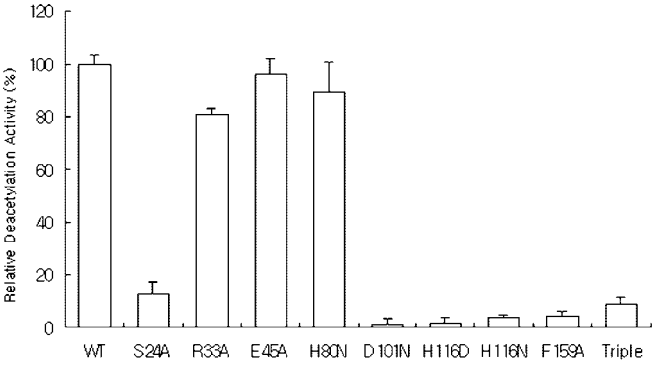

FIG. 2. **NAD-dependent deacetylase assays.** Reactions contained either wild type Sir2-Af1 or one of the mutants, ^{3}H-acetylated, recombinant BSA, and 500 μM NAD. Release of acetate from the labeled substrate was quantified as described under "Experimental Procedures." *Error bars* denote S.D. from mean value.

the replacement of His-116 with either Asp or Asn reduced the activity 30–50-fold, suggesting that this residue has a key catalytic role. His-116 formed a hydrogen bond to the O3′ of NAD, and this interaction was observed in all three structural forms. The removal of the aromatic ring from Phe-159 also dramatically reduced the activity. Although the side chain is close to the ribose ring (3.4 Å from O1), it did not make any direct interactions with NAD, and its side chain was partly buried (~50%).

To find out more about the role of Phe-159, we examined the kinetic parameters of wild type Sir2-Af1 and the F159A mutant (Table II). The K_m value of the mutant enzyme was twice that of wild type enzyme, whereas the k_{cat} was 5-fold less. When we compared the structures of the open and closed form of Sir2, we found that the ring of Phe-159 was directed to the surface of the molecule in the open conformation, whereas it was rotated about 180° toward the active site in the closed form (Fig. 1*c*). Interestingly, in the crystals of the closed form, the extra four residues in a symmetry-related molecule occupied a surface crevice formed by His-116, Phe-159, and Val-190 near the nicotinamide ribose, suggesting that they may be mimicking substrate binding. Indeed, the interaction between the extra four residues in the C terminus and the surface crevice in a neighboring Sir2 molecule was one of the major interactions observed within the crystal. Because Sir2 is a monomer in solution, this Sir2-Sir2 interaction may not be biologically relevant. Nevertheless, this packing suggests that the surface crevice does have structural properties, indicating that it is a substrate binding site. Together with the kinetic data, this suggests that Phe-159 may guide the substrate into the correct position in the active site during catalysis. When we have determined the structure of Sir2 containing the F159A mutation, despite the abrogation of enzymatic activity in the mutant protein, we did not observe any noticeable local changes in the structure of the mutant compared with wild type Sir2-Af1. The root mean square deviations for all Cα atoms were 0.4 Å between two structures, and the Cα for the Phe-159 residue deviated 0.5 Å. In the F159A mutant, two water molecules occupied the position of the Phe-159 ring.

Analysis of Mutations at Site C—We also examined the role of residues located at the core region in site C. Ser-24 and Asp-101 are deeply buried, to stabilize the floor for the adenine base and adenine ribose of NAD, and are hydrogen-bonded to each other. Mutation of a residue in yeast HST1 that is equivalent to Ser-24 in Sir2-Af1 completely abolished histone deacetylase activity (17), and it has been proposed that this residue may be involved in the cleavage of the glycosidic linkage between nicotinamide and ribose (17). In contrast to these

TABLE II
Kinetic parameters for protein deacetylation by Sir2

	K_m	k_{cat}	k_{cat}/K_m
	μM	s^{-1}	$s^{-1}\ \mu M^{-1}$
Wild type	2.12 ± 0.35	0.235 ± 0.027	0.1109 ± 0.0367
F159A	3.94 ± 0.74	0.053 ± 0.011	0.0135 ± 0.0058

data, we find that Ser-24 to Ala and Asp-101 to Asn mutations in Sir2-Af1 decreased the enzymatic activity by 6- and 80-fold, respectively. This suggests that Ser-24 is not essential for deacetylase activity. The distance between the OH group of Ser-24 and the O_2' of nicotinamide ribose is 12.5 Å, and the distance for the OD2 group of Asp-101 is 10.9 Å to the O_2' of nicotinamide ribose. Because a significant portion of the side chains of Ser-24 and Asp-101 is buried, the activity decrease may be due to decreased stability of the protein.

To address this possibility, we determined the T_m of the wild type and mutant proteins. This analysis revealed that the T_m value of the S24A mutant was 95 °C, a decrease of 3 °C compared with the wild type. The T_m of Asn-101 mutant was decreased by 10 °C (Fig. 3*a*). We also analyzed the effects of mutation of His-80 on the activity and T_m Sir2-Asf1. In our structures, the side chain of His-80 was completely buried, interacting directly with Ser-24 and with Asn-99 and Asp-101 via a water molecule. Interestingly, the His-80 to Asn-80 mutant retained significant activity, although its T_m was decreased by about 10 °C. Although the 10 °C reduction in T_m of some mutants was considerable in terms of protein stability, it must be stressed that the T_m values for these mutants were all much higher than the temperature at which activity was measured. One interpretation of these data is that residues such as Asp-101 and Ser-24 may be directly involved in catalysis. Alternatively, since our stability analysis only accounts for the global stability, we cannot rule out the possibility that the mutant structures are locally perturbed and that this could cause the decrease in enzyme activity either by affecting binding of NAD or substrate.

To further address this issue, we measured the binding affinities of NAD to the wild type and mutant Sir2 proteins using isothermal titration calorimetry. As seen in the Table III, H80N Sir2 retained about 60% of the NAD binding ability of wild type Sir2. However, the NAD binding constants of the S24A and D101N Sir2 proteins were decreased 9–10-fold. Thus, the NAD binding assay data suggest that the decreased NAD-dependent deacetylase activities for the S24A and D101N mutant proteins are at least partly due to reduced binding affinities for NAD.

To understand these observations at structural level, we determined the structures of Sir2-Af1 S24A and Sir2-Af1 H80N and compared these with the wild type structure (Table I; Fig. 3*b*). In Sir2-Af1 S24A, a buried water molecule that mediates the interactions of Ser-24, His-80, Asn-99, and Asp-101 moved slightly (0.3 Å) toward the mutated Ala residue and linked the three residues His-80, Asn-99, and Asp-101. No other local changes were observed in this mutant structure.

In the structure of Sir2-Af1 H80N, the hydrogen bond between His-80 and Ser-24 was broken. Instead, a water molecule was introduced and mediated the interaction between the two residues via a hydrogen bond. Consequently, the conserved water molecule that connects three residues was relocated toward the Asn-99, forming a hydrogen bond with the newly added water (Fig 3*b*). In the wild type structure, His-80 also contacts Asp-101 via a water molecule. The same water-mediated interaction is also conserved in H80N. Therefore, it is unlikely that the alteration of His-80 perturbs the interactions between NAD and residues in the binding pocket. This finding

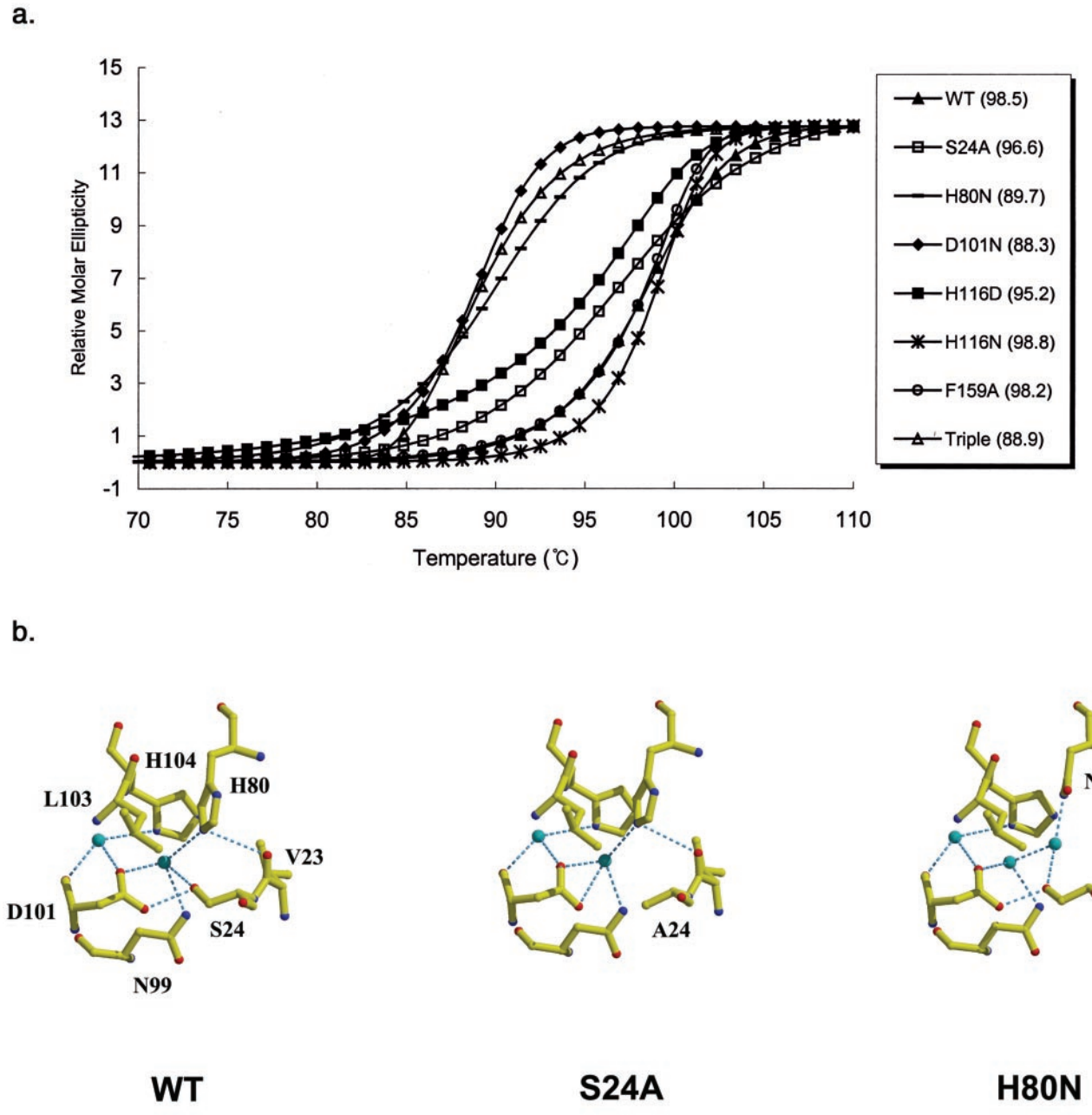

FIG. 3. *a*, thermal melting curves of wild type (*WT*) and mutant Sir2-Af1 determined by circular dichroism. A summary of T_m values is given on the right for each protein listed inside the parenthesis. The unit (°C) is omitted for clarity. *b*, local conformational changes in the site C upon mutation. The wild type (*left*), Ser-24 to Ala (*middle*), and His-80 to Asn (*right*) structures are shown as *ball-and-stick* models. The carbon atoms are shown in *yellow*, oxygen atoms are shown in *red*, nitrogen atoms are shown in *blue*, and water molecules are shown in *cyan*.

TABLE III
Binding affinities of NAD to wild type and mutant Sir2 proteins

	Dissociation constant, K_d
	μM
Wild type	81.04 ± 11.11
S24A	719.94 ± 157.54
H80N	142.1 ± 34.47
D101N	798.7 ± 194.16

is in agreement with the minor effect of the H80N mutation on enzyme activity and NAD binding (Fig. 3*b*).

The decrease of the T_m by 10 °C in the Asn-101 mutant is significant considering that Asp is replaced by its stereoisomer, Asn. Although we have not succeeded in obtaining crystals of this mutant, it seems likely that the replaced ND1 of Asn-101 perturbs the hydrogen bond between Ser-24 and Asp-101 and thereby affects the local structure in this region. Such local destabilization may affect the location of Gln-98, which has a conserved interaction with O3′ of nicotinamide ribose in all forms of the Sir2 structure. Thus, the structures of the Sir2 derivatives with mutations in site C reveal a correlation between local structural alterations and severity of impairment of enzyme activity. The local structural alterations are likely to impinge on the binding of NAD within the pocket. Taken together, these data suggest that the site C residues play a role in substrate binding and positioning rather than a direct role in catalysis.

Formation of 2′-O-Acetyl ADP-ribose in the Active Site—One of our mutants, the triple mutant, crystallized in hexagonal I form, $P3_2$. We were unable to grow this form of crystal

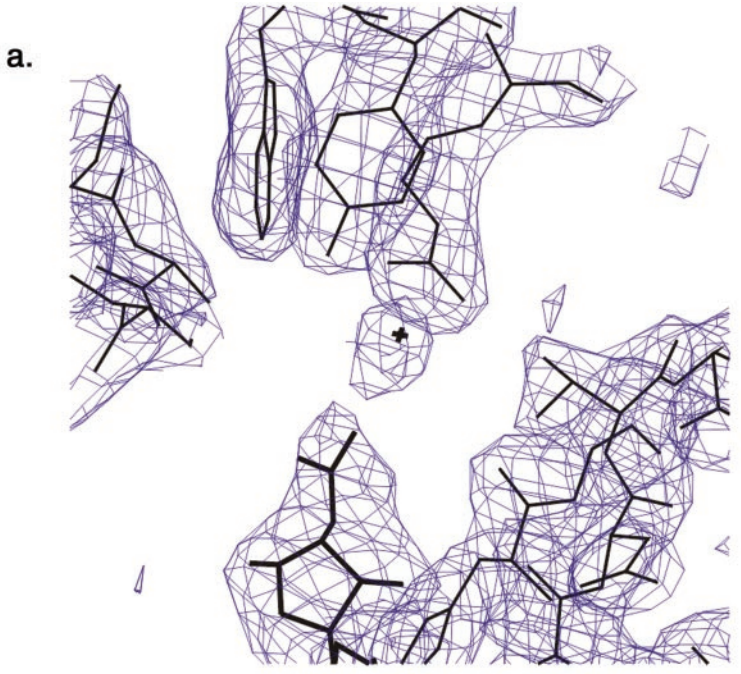

FIG. 4. *a*, a 2.6-Å $2F_o - F_c$ map showing the region around the 2′-*O*-acetyl ADP-ribose in the triple mutant of Sir2-Af1. The map is contoured at 1.4 σ. *b*, a stereo diagram showing the interactions between 2′-*O*-acetyl ADP-ribose and residues in the active site of the triple mutant of Sir2-Af1.

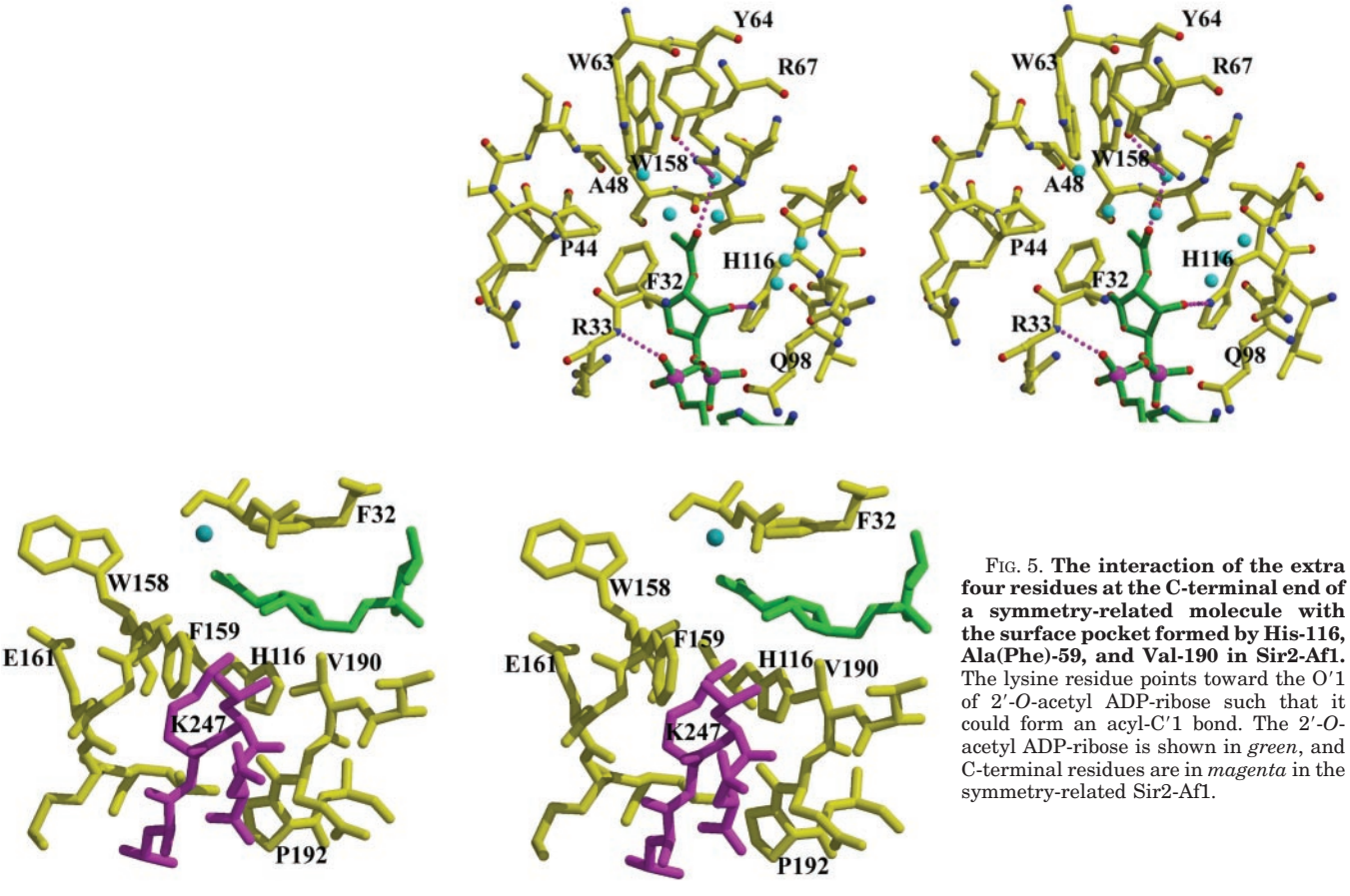

FIG. 5. **The interaction of the extra four residues at the C-terminal end of a symmetry-related molecule with the surface pocket formed by His-116, Ala(Phe)-59, and Val-190 in Sir2-Af1.** The lysine residue points toward the O′1 of 2′-*O*-acetyl ADP-ribose such that it could form an acyl-C′1 bond. The 2′-*O*-acetyl ADP-ribose is shown in *green*, and C-terminal residues are in *magenta* in the symmetry-related Sir2-Af1.

from any other mutants. The crystal contained about 70% solvent, and this could limit the diffraction of crystals. When we added an excess of *N*-acetyl lysine to the crystal, the space group of the crystal was changed to $P3_121$, and the *c* axis of the unit cell dimension was elongated 2-fold, giving the hexagonal II form. When these two structures were compared, no significant differences were observed in overall structure (root mean square deviations of 0.67 Å with a maximum deviation of 3.2 Å for all Cα atoms). Strikingly, however, we observed a clear density for an acetyl group at the O_2' posi-

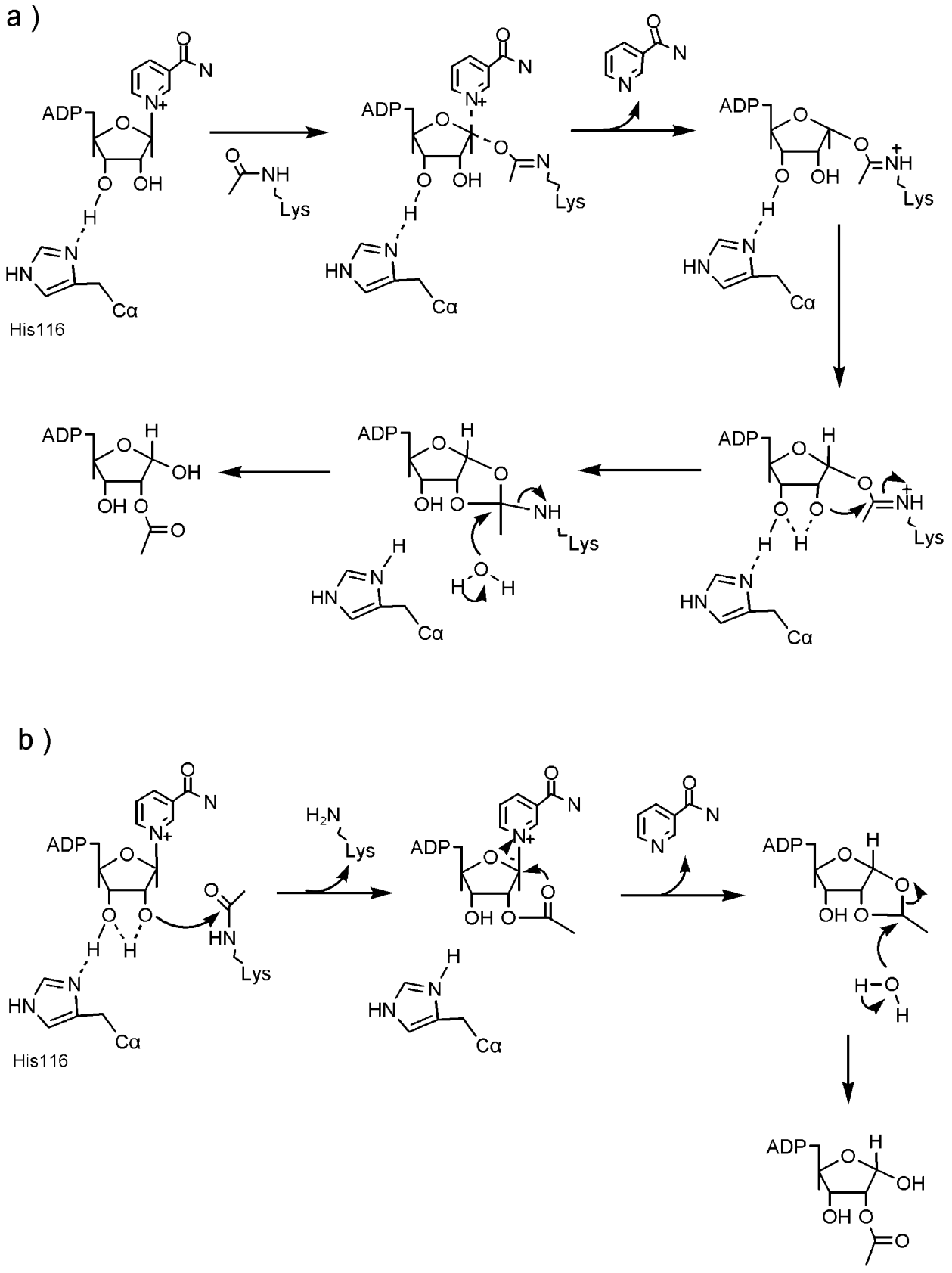

FIG. 6. **Proposed mechanism for the transfer of acetyl group to NAD by Sir2 to generate 2′-*O*-acetyl-ADP-ribose.** *a*, the carbonyl oxygen of N-acetyl lysine binds to the C1′ of nicotinamide ribose, forming a O1′ amidate intermediate followed by the release of nicotinamide ring. The intramolecular attack by the activated 2′-OH on carbonyl carbon generates the acyloxonium ion. His-116 deprotonates the 2′-OH directly or indirectly through 3′-OH activation. The resulting 1′,2′-acyloxonium ion reacts with a water molecule to form 2′-*O*-acetyl ADP-ribose. *b*, the activated 2′-OH of nicotinamide ribose attacks the carbonyl carbon of the substrate, and the lysine group is released. The carbonyl oxygen makes an intramolecular attack on the C1′ to hydrolyze the glycosidic bond between ribose and nicotinamide and generate the reactive 1′,2′-acyloxonium ion, that is converted to the product, as in panel *a*.

tion of nicotinamide ribose and for a closely located water (Fig. 4*a*). The 2′-*O*-acetyl ADP-ribose had a generally similar binding mode to ADP-ribose. New interactions were observed between the oxygen atom of the acetyl group and the side chains of Tyr-64 and Arg-67 via a water molecule (Fig. 4*b*). The distances between the water molecule and the acetyl oxygen, OH group of Tyr-64, and NH1 group of Arg-67 were 2.7, 3.0, and 3.1 Å, respectively. The ND1 of His-116 was 3.0 Å away from the O3′ of the nicotinamide ribose. The methyl group of the acetyl group was surrounded by Phe-32, Ala-48, Trp-158, and Ala-159 (Phe-159). Intriguingly, the extra four residues at the C-terminal end of a symmetry-related molecule bound to the surface pocket of Sir2 formed by His-116, Ala (Phe)-59, and Val-190, positioning the Lys-248 near the O1′ of the nicotinamide ribose and yielding similar interactions to those seen in the closed form crystal (Fig. 5). Our observation of the formation of 2′-*O*-acetyl ADP-ribose on the active site of Sir2 allows us to propose a revised catalytic mechanism, as described below. While this manuscript was in preparation, NMR studies were reported that the regioisomer of 2′- and 3′-*O*-acetyl ADP-ribose is the product of NAD-dependent histone deacetylase reaction, thus confirming our results (23, 24). When released from the active site, we predict that the 2′-*O*-acetyl ADP-ribose product is converted to 3′-*O*-acetyl ADP-ribose, leading to establishment of an equilibrium between these two isomers.

Acetyl Group Transfer Mechanism—The importance of NAD-dependent deacetylation by Sir2 can be divided 2-fold. The deacetylation on N-terminal tails of histones or other proteins such as p53 modulates the gene expression or apoptosis. Second, a new metabolite produced by Sir2 reaction may be involved in an unknown cellular-signaling pathway. Indeed, the Sir2 reaction product causes a delay or block in oocyte cell division (19). Alternatively, the product may be required for a novel modification reaction in which the transfer of an acetyl group is involved. Considering the significance of Sir2 and its final product in diverse events including the aging process, it is important to elucidate how Sir2 catalyzes the reaction and to identify the final product of this reaction. Our structural and mutational information and identification of reaction products in conjunction with NMR studies (23, 24) allow us to elucidate the catalytic mechanisms of the reaction (Fig. 6, *a* and *b*), and because Sir2 is conserved across phylogenetic domains, we presume the mechanism proposed here is generally applicable to other homologues (13).

First, upon entrance into the active site of Sir2, the acyl oxygen of *N*-acetyl lysine attacks the C1′ of the nicotinamide ribose ring. This interaction generates 1′-*O*-alkylamidate and releases nicotinamide. Subsequently, the activated hydroxyl group at C2′ makes a nucleophilic attack on the carbon of the amide carbonyl. This leads to the formation of an unstable 1′,2′-cyclic acyloxonium ion. How is the 2′-OH group activated? One possibility is that it is activated indirectly by His-116 in site B. The 3′-OH that is hydrogen-bonded to the ND1 of His-116 is deprotonated and consequently activates the 2′-OH. It is also possible that substrate binding to Sir2 slightly perturbs the position of His-116, allowing direct activation of the 2′-OH by His-116. Finally, although the primary role of Asp-101 in site C is to stabilize the local structure, we cannot completely exclude the possibility that this residue may act as a base in the deprotonation of 2′-OH or 3′-OH (Fig. 6*b*). However, in this case, a gross movement around the phosphodiester bond of NAD combined with the rearrangement of the positions of Tyr-64 and Arg-67, loop containing residues 30–36, and residues around Gly-20 and Ala-21 would be required to place the 2′-OH in the deprotonation range of residues in C site. The acid exchange experiment of Sauve *et al.* (23) suggests that the solvent oxygen atom is incorporated into nicotinamide ribose and resides in the acetate moiety. These data indicate, therefore, that a water molecule is involved in the attack on the amide carbon of the 1′,2′-cyclic acyloxonium ion with concomitant release of the lysine group. The combination of these data together with our structural and functional results lead us to propose that a water molecule may be activated by residues in site B, or because the cyclic acyloxonium ion is unstable, a water molecule may directly attack the oxonium ion.

In an alternative mechanism, the acetyl oxygen is positioned optimally so that the 2′-OH activated by His-116 acts directly as a nucleophile on the carbonyl carbon of N-acetyl lysine, followed by the release of lysine. This leads to the formation of 2′-acetyl NAD. The carbonyl carbon in 2′-acetyl NAD attacks the C1′ to release the nicotinamide, with the formation of 1′,2′-cyclic acyloxonium. The activated water molecule would then react to form the 2′-*O*-acetyl ADP-ribose. In both mechanisms, the 2′-*O*-acetyl ADP-ribose would be released from the active site of the enzyme and converted to 3′-*O*-acetyl ADP-ribose.

It has been shown that the nicotinamide-NAD exchange catalyzed by Sir2 occurs only in the presence of the protein substrate (33). The two proposed mechanisms clearly explain this observation. However, the correlation between the 2′-OH activation and nicotinamide release requires further experimental data. In the first mechanism, the 2′-OH activation and nicotinamide exchange are separate processes, whereas they are coupled in the second mechanism. In yeast Sir2 homologue, HST1, the Ser-24 to Ala mutant failed to show exchange between the nicotinamide and NAD (17). That the S24A mutant in yeast Sir2 did not have any activity (although this contrasts with our findings on S24A of Af1-Sir2) could support the second mechanism we propose. By contrast, His-116A mutant in yeast Sir2, which is also inactive in deacetylation, did show some exchange between nicotinamide and NAD, suggesting that the first mechanism is more likely to occur.

In summary, we have provided crystallographic evidence that 2′-*O*-acetyl ADP-ribose is a final product in the Sir2 reaction and propose a revised mechanism for catalysis based on the structural and functional characterization of Sir2 mutants. In our mechanism, the activation of the 2′-OH of nicotinamide ribose by His-116 is essential for the hydrolysis of the acetyl groups from *N*-acetyl lysine. The conserved Ser-24 and Asp-101 participate in the stabilization of local structure for NAD binding rather than direct involvement in catalysis. The structural information for the 2′-*O*-acetyl ADP-ribose-Sir2 complex and the proposed mechanism should help to guide the design of inhibitors that would allow the control of Sir2-dependent events including cell cycle, DNA damage signaling, and aging processes. Furthermore, such inhibitors could be used to understand the broad functions of Sir2 and its homologues and elucidate novel signal transduction pathways where Sir2 is involved.

Acknowledgments—We thank Y. G. Yu for the generous gift of chromosomal DNA from *A. fulgidus*. We also thank J. Bradbury for critical reading, B. H. Oh for helpful suggestions, and the members of Pohang Acceleratory Laboratory for help in data collection.

REFERENCES

1. Imai, S., Armstrong, C. M, Kaeberlein, M., and Guarente, L. (2000) *Nature* **403,** 795–800
2. Smith, J. S., Brachmann, C. B., Celic, I., Kenna, M. A., Muhammad, S., Starai, V. J., Avalos, J. L., Escalante-Semerena, J. C., Grubmeyer, C., Wolberger, C., and Boeke, J. D. (2000) *Proc. Natl. Acad. Sci. U. S. A.* **97,** 6658–6663
3. Landry, J., Sutton, A., Tafrov, S. T., Heller, R. C., Stebbins, J., Pillus, L., and Sternglanz, R. (2000) *Proc. Natl. Acad. Sci. U. S. A.* **97,** 5807–5811

4. Moazed, D. (2001) *Mol. Cell* **8,** 489–498
5. Tanny, J. C., Dowd, G. J., Huang, J., Hilz, H., and Moazed, D. (1999) *Cell* **99,** 735–745
6. Gottschling, D. E., Aparicio, O. M., Billington, B. L., and Zakian, V. A. (1990) *Cell* **63,** 751–762
7. Smith, J. S., and Boeke, J. D. (1997) *Genes Dev.* **11,** 241–254
8. Kaeberlin, M., McVey, M., and Guerente, L. (1999) *Genes Dev.* **13,** 2570–2580
9. Hecht, A., Laroche, T., Strahl-Bolsinger, S., Gasser, S. M., and Grunstein, M. (1995) *Cell* **80,** 583–592
10. Defossez, P. A., Park, P. U., and Guarente, L. (1998) *Curr. Opin. Microbiol.* **1,** 707–711
11. Tissenbaum, H. A., and Guarente, L. (2001) *Nature* **8,** 227–230
12. Guarente, L. (2001) *Genes Dev.* **14,** 1021–1026
13. Frye, R. A. (2000) *Biochem. Biophys. Res. Commun.* **273,** 793–798
14. Bell, S. D., Botting, C. H., Wardleworth, B. N., Jackson, S. P., and White, M. F. (2002) *Science* **296,** 148–151
15. Vaziri, H., Dessain, S. K., Eaton, E., Imai, S. I., Frye, R. A., Pandita, T. K., Guarente, L., and Weinberg, R. A. (2001) *Cell* **107,** 149–159
16. Luo, J., Nikolaev, A. Y., Imai, S., Chen, D., Su, F., Shiloh, A., Guarente, L., and Gu, W. (2001) *Cell* **107,** 137–148
17. Min, J., Landry, J., Sternglanz, R., and Xu, R. M. (2001) *Cell* **105,** 269–279
18. Grozinger, C. M., Chao, E. D., Blackwell, H. E., Moazed, D., and Schreiber, S. L. (2001) *J. Biol. Chem.* **276,** 38837–38843
19. Borra, M. T., O'Neill, F. J., Jackson, M. D., Marshall, B., Verdin, E., Foltz, K. R., and Denu, J. M. (2002) *J. Biol. Chem.* **277,** 12632–12641
20. Finnin, M. S., Donigian, J. R., and Pavletich, N. P. (2001) *Nat. Struct. Biol.* **8,** 621–625
21. Tanner, K. G., Landry, J., Sternglanz, R., and Denu, J. M. (2000) *Proc. Natl. Acad. Sci. U. S. A.* **97,** 14178–14182
22. Tanny, J. C., and Moazed, D. (2001) *Proc. Natl. Acad. Sci. U. S. A.* **98,** 415–420
23. Sauve, A. A., Celic, I., Avalos, J., Deng, H., Boeke, J. D., and Schramm, V. L. (2001) *Biochemistry* **40,** 15456–15463
24. Jackson, M. D., and Denu, J. M. (2002) *J. Biol. Chem.* **277,** 18535–18544
25. Stetter, K. O. (1988) *Syst. Appl. Microbiol.* **10,** 172–173
26. Klenk, H.-P., Venter, J. C., *et al.* (1997) *Nature* **390,** 364- 370
27. Otwinowski, Z., and Minor, W. (1997) *Methods Enzymol.* **276,** 307–326
28. Collaborative Computational Project B (1994) *Acta Crystallogr. Sect. D Biol. Crystallogr.* **50,** 760–763
29. Sack, J. S. (1988) *J. Mol. Graph.* **6,** 224–225
30. Jones, T. A., Zou, J.-Y., Cowan, S. W., and Kjeldgaard, M. (1991) *Acta Crystallogr. Sect. A* **47,** 110–119
31. Brunger, A. T., Adams, P. D., Clore, G. M., DeLano, W. L., Gros, P. Grosse-Kunstleve, R. W., Jiang, J. S., Kuszewski, J., Nilges, M., Pannu, N. S., Read, R. J., Rice, L. M, Simonson, T., and Warren, G. L. (1998) *Acta Crystallogr. Sect. D Biol. Crystallogr.* **54,** 905–921
32. Letherbarrow, R. J. (1987) *ENZFITTER: A Nonlinear Regression Data Analysis Program for the IBM PC/P 52*, Elsevier Biosoft, Cambridge, United Kingdom
33. Landry, J., Slama, J. T., and Sternglanz, R. (2000) *Biochem. Biophys. Res. Commun.* **278,** 685–690
34. Kraulis, P. J. (1991) *J. Appl. Crystallogr.* **24,** 946–950
35. Merrit, E. A., and Murphy, M. E. P. (1994) *Acta Crystallogr. Sect. D Biol. Crystallogr.* **50,** 869–873